Journal of Materials Chemistry C

ROYAL SOCIETY OF CHEMISTRY

PAPER

View Article Online
View Journal | View Issue

Cite this: J. Mater. Chem. C, 2021, 9, 2001

Synthesis of spirodithienogermole with triphenylamine units as a dopant-free hole-transporting material for perovskite solar cells†

Joji Ohshita, *[ab] Keisuke Kondo,[a] Yohei Adachi, [a] Myungkwan Song *[c] and Sung-Ho Jin *[d]

Received 15th October 2020,
Accepted 7th January 2021

DOI: 10.1039/d0tc04905k

rsc.li/materials-c

Spiro-condensed dithienogermoles with electron-donating aromatic substituents were prepared by Pd-catalyzed Stille coupling reactions of spirobi(dibromodithienogermole) and the corresponding trimethylstannylarene derivatives. Their optical and electrochemical properties were examined in comparison with those of related model compounds without the germole ring systems and the spiro-condensed unit, indicating that the spiro-condensed dithiengermole systems play roles in the enhancement of the conjugation. Perovskite solar cells (PSCs) were fabricated using triphenylamine-containing spirobi(dithienogermole) (**sDTG-tpa**) as the hole-transporting material (HTM). The PSCs showed the maximal photo-current conversion efficiency of 14.67%, which was higher than that of a similar device with **spiro-OMeTAD** as the HTM (9.53%), indicating the superior performance of **sDTG-tpa** as HTM compared with **spiro-OMeTAD**, a typical HTM for PSCs.

1 Introduction

Perovskite solar cells (PSCs) have attracted growing interest because of their high performance. In a typical PSC system, a mesoporous TiO_2 photoanode, a perovskite light absorption material, a hole-transporting material (HTM), and a cathode are layered on an FTO electrode in this order. Many types of organic conjugated molecules and polymers have been studied as HTMs.[1–3] Of these, spiro-condensed fluorene derivative **spiro-OMeTAD**[3] (Chart 1) has been widely used as a typical HTM for PSCs because it shows sufficient solubility in organic solvents, thereby providing high processability, and can form a thermally stable amorphous phase likely due to its spiro-condensed molecular structure. PSCs with high photo-current conversion efficiencies (PCEs) have been prepared using **spiro-OMeTAD**. However, the hole mobility of **spiro-OMeTAD** is not very high and therefore, additives and dopants are often used to improve PSC performance.[3,4] To improve the performance of **spiro-OMeTAD** as HTM, its chemical modification has been investigated.[3] For example, **spiro-CPDT** with bithiophene units in place of the fluorene units in **spiro-OMeTAD** was prepared and found to possess high hole-transporting property, thereby enabling its use as a dopant-free HTM for PSCs.[5] Development of dopant-free HMT is desired to simplify the process, to reduce the cost, and to improve the reproducibility of cell fabrication, and therefore further studies to develop new molecular system for new HTMs with even higher performance are required.

On the other hand, element-bridged biaryl systems have been studied extensively as new molecular motifs of organic electronic materials whose electronic states and properties can be finely controlled by the choice of the bridging element.[6] Of

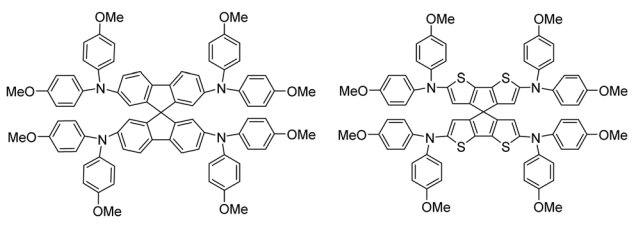

Chart 1 Spiro compounds used as typical HTMs for PSCs.

[a] Applied Chemistry Program, Graduate School of Advanced Science and Engineering, Hiroshima University, Higashi-Hiroshima 739-8527, Japan. E-mail: jo@hiroshima-u.ac.jp
[b] Division of Materials Model-Based Research, Digital Monozukuri (Manufacturing) Education and Research Center, Hiroshima University, Higashi-Hiroshima 739-0046, Japan
[c] Materials Center for Energy Convergence, Surface Technology Division, Korea, Institute of Materials Science (KIMS), 797 Changwondaero, Sungsan-Gu, Changwon, Gyeongnam 642-831, Republic of Korea. E-mail: smk1017@kims.re.kr
[d] Department of Chemistry Education, Graduate Department of Chemical Materials, Institute for Plastic Information and Energy Materials, Pusan National University, Busandaehakro 63-2, Busan 46241, Republic of Korea. E-mail: shjin@pusan.ac.kr

† Electronic supplementary information (ESI) available: NMR spectra and CVs of the presently prepared compounds, simulated HOMO and LUMO profiles of **sDTG-tpa**, and optimized geometry of **sDTG-tpa**. See DOI: 10.1039/d0tc04905k

these, dithienometallole derivatives are of current interest as functional materials and those with group 14 heavy elements, such as Si, Ge, and Sn, have been applied as organic electronic materials for organic light emitting diodes, organic field-effect transistors, and photovoltaic cells.[7] Because of the high planarity of the tricyclic system, dithienometalloles show enhanced conjugation. In addition, it has been suggested that the introduction of these heavy elements enhances intermolecular interaction to improve the carrier transporting properties of these compounds in their films.[8] Recently, a dithienosilole-based linearly-conjugated compound was prepared as a new dopant-free HTM for PSCs.[9] In this work, we designed and prepared spirobi(dithienogermole)s with electron-donating aromatic substituents as new HTMs. Their optical and electrochemical properties were investigated, indicating that the spiro-condensed dithiengermole systems play roles in enhancing the conjugation. Of the spirobi(dithienogermole)s thus prepared, that with four triphenylamine substituents (**sDTG-tpa**) was applied as the HTM for PSCs and the compound showed higher performance than **spiro-OMeTAD** in PSCs.

2 Experimental

2.1 General

All reactions were carried out in dry argon. Toluene used as reaction solvent was distilled from calcium hydride and stored over activated molecular sieves under argon until use. Usual workup mentioned below includes hydrolysis of the reaction mixture with water, separation of the organic layer, washing the organic layer twice with water, drying the organic layer over anhydrous magnesium sulfate, and evaporation of the solvent in this order.

NMR spectra were recorded on Varian System 500 and 400MR spectrometers (Fig. S1–S5, ESI†). High-resolution mass spectra were obtained on a Thermo Fisher Scientific LTQ Orbitrap XL spectrometer at N-BARD, Hiroshima University. Preparative gel permeation chromatography (GPC) was performed on serially connected Shodex KF2001 and KF2002 columns using toluene as eluent. UV-vis ABS and PL spectra were measured on HITACHI U-2910 and HORIBA FluoroMax-4 spectrophotometers, respectively. CVs were obtained on a Hokuto Denko automatic polarization system Hz-7000 with 1.0 mM DMF solutions containing 100 mM TBAP as supporting electrolyte and using Pt wire, Pt plate, and Ag/Ag^+ electrode as the working, counter, and reference electrodes, respectively.

2.2 Preparation of sDTG-tpa

A mixture of 0.705 g (0.984 mmol) of spirobi(dibromodithienogermole), 3.00 g (6.89 mmol) of *N*,*N*-diphenyl-4-(trimethylstannyl)aniline, 69.2 mg (58.5 μmol, 5 mol%) of $Pd(PPh_3)_4$, and 60 mL of toluene was heated to reflux for 48 h. After usual workup, the residue was subjected to silica gel column chromatography using hexane : dichloromethane = 1 : 1 as eluent to give 3.17 g of the crude product, a portion of which (0.501 g) was purified by preparative GPC to provide 0.0470 g (0.0342 mmol, 22% yield) of **sDTG-tpa** as a yellow solid. ^{1}H NMR (in $CDCl_3$, 500 MHz): δ = 7.02–7.06 (16H, m, phenylene and phenyl), 7.11 (16H, br d, phenyl, J = 7.6 Hz), 7.17 (4H, s, DTG), 7.26 (16H, br t, phenyl, J = 7.8 Hz), 7.42 (8H, d, phenylene, J = 8.7 Hz). ^{13}C NMR (in $CDCl_3$, 100 MHz): δ = 123.30, 123.68, 124.73, 125.04, 126.45, 126.34, 129.47, 136.48, 146.06, 147.20, 147.37, 147.54. HR-MS (APCI) Calcd for $C_{88}H_{60}N_4GeS_4$ [M^+]: 1374.29071; found: 1374.29468. m.p. > 300 °C.

2.3 Preparation of sDTG-dmap

A mixture of 0.306 g (0.427 mmol) of spirobi(dibromodithienogermole), 0.605 g (2.13 mmol) of *N*,*N*-dimethyl-4-(trimethylstannyl)aniline, 26.7 mg (23.1 μmol, 5 mol%) of $Pd(PPh_3)_4$, and 30 mL of toluene was heated to reflux for 21 h. After usual workup, the residue was subjected to silica gel column chromatography using hexane : dichloromethane = 1 : 1 as eluent to provide 83.0 mg (94.5 μmol, 20% yield) of **sDTG-dmap** as an orange solid. ^{1}H NMR (in $CDCl_3$, 400 MHz): δ = 2.97 (24H, s, methyl), 6.70 (8H, d, phenyl, J = 8.9 Hz), 7.11 (4H, s, DTG), 7.45 (8H, d, phenyl, J = 8.9 Hz). ^{13}C NMR (in $CDCl_3$, 100 MHz): δ = 40.59, 112.72, 123.07, 123.76, 126.70, 136.19, 146.26, 146.58, 149.99. HR-MS (APCI) calcd for $C_{48}H_{44}GeN_4S_4$ [M^+]: 878.16551; found: 878.16477. m.p. 169–170 °C.

2.4 Preparation of sDTG-mop

A mixture of 0.187 g (0.261 mmol) of spirobi(dibromodithienogermole), 0.346 g (1.277 mmol) of 4-(trimethylstannyl)anisole, 15.0 mg (13.0 μmol, 5 mol%) of $Pd(PPh_3)_4$, and 10 mL of toluene was heated to reflux for 30 h. After usual workup, the residue was subjected to silica gel column chromatography using hexane : dichloromethane = 3 : 5 as eluent to provide 19.0 mg (23.0 μmol, 9% yield) of **sDTG-mop** as a yellow solid. ^{1}H NMR (in $CDCl_3$, 500 MHz): δ = 3.82 (12H, s, methoxy), 6.89 (8H, d, phenyl, J = 8.9 Hz), 7.15 (4H, s, thiophene), 7.50 (8H, d, phenyl, J = 8.9 Hz). ^{13}C NMR (in $CDCl_3$, 125 MHz): δ = 55.48, 114.52, 124.91, 126.99, 127.26, 136.29, 146.00, 147.12, 159.33. HR-MS (APCI) Calcd for $C_{44}H_{32}GeO_4S_4$ [M^+]: 826.03897; found: 826.04032. M.p. > 300 °C.

2.5 Preparation of m1

A mixture of 96.0 mg (0.133 mmol) of tetrakis(4-bromo-2-thienyl)germane, 0.228 g (0.559 mmol) of *N*,*N*-diphenyl-4-(trimethylstannyl)aniline, 9.8 mg (8.5 μmol, 5 mol%) of $Pd(PPh_3)_4$, and 10 mL of toluene was heated to reflux for 30 h. After usual workup, the residue was subjected to silica gel column chromatography using hexane : dichloromethane = 1 : 1 as eluent, followed by further purification by preparative GPC to provide 22.0 mg (16.0 μmol, 12% yield) of **m1** as a colorless solid. ^{1}H NMR (in $CDCl_3$, 400 MHz): δ = 7.04 (8H, br t, phenyl, J = 7.0 Hz), 7.06 (8H, d, phenylene, J = 8.8 Hz), 7.11 (16H, br d, phenyl, J = 7.5 Hz), 7.24–7.29 (16H, m, phenyl), 7.36 (4H, d, thiophene, J = 3.6 Hz), 7.42 (4H, d, thiophene, J = 3.6 Hz), 7.50 (8H, d, phenylene, J = 8.8 Hz). ^{13}C NMR (in $CDCl_3$, 100 MHz): δ = 123.27, 123.65, 123.75, 124.68, 127.09, 128.30, 129.45, 132.25, 137.54, 147.61, 147.68, 151.40. HR-MS (APCI) calcd for $C_{88}H_{64}GeN_4S_4$ [M^+]: 1378.32201; found: 1378.32605. M.p. > 300 °C.

2.6 Preparation of m2

A mixture of 77.0 mg (0.140 mmol) of dibromodiphenyldithienogermole, 0.117 g (0.287 mmol) of *N*,*N*-diphenyl-4-(trimethylstannyl)aniline, 9.7 mg (8.4 μmol, 5 mol%) of $Pd(PPh_3)_4$, and 10 mL of toluene was heated to reflux for 22 h. After usual workup, the residue was subjected to silica gel column chromatography using hexane : dichloromethane = 3 : 1 as eluent to provide 53.7 mg (61.2 μmol, 45% yield) of **m2** as a yellow solid. ^{1}H NMR (in $CDCl_3$, 400 MHz): δ = 7.05 (4H, d, phenylene, J = 8.9 Hz), 7.08–7.13 (12H, m, phenyl), 7.33 (8H, dd, phenyl, J = 7.4, 7.2 Hz), 7.42–7.48 (6H, m, phenyl), 7.64 (4H, d, phenylene, J = 8.9 Hz), 7.68-7.71 (4H, m, phenyl), 7.74 (2H, s, thiophene). ^{13}C NMR (in $CDCl_3$, 100 MHz): δ = 123.55, 124.26, 124.96, 125.23, 126.85, 129.08, 129.12, 129.78, 130.31, 134.53, 135.16, 141.75, 146.09, 146.82, 147.58, 147.97. HR-MS (APCI) Calcd for $C_{56}H_{40}GeN_2S_2$: $[M + H]^+$: 878.18392; found: 878.18616. M.p. 55.4–57.8 °C.

2.7 Materials for device fabrication

Methylammonium iodide (MAI, CH_3NH_3I) was synthesized with 13.93 mL methylamine (40% in methanol, TCI) and 15 mL of hydroiodic acid (57 wt% in water, Aldrich) in a 250 mL round bottom flask at 0 °C for 4 h stirring. The precipitate was generated by evaporation at 70 °C for 30 min. The product, CH_3NH_3I was recrystallized 3 times from an ethanol solution and washed 5 times with diethyl ether. Finally, the resultant white powder was dried in a vacuum oven for overnight at 65 °C. Lead(II) iodide (PbI_2) (99.99%) was purchased from Alfa Aesar. Spiro-OMeTAD (99.5%), obtained from Lumtec (Taiwan). Titanium diisopropoxide dis(acetylacetonate) and $TiCl_4$ (98%) were obtained from Sigma Aldrich (Korea). Acetonitrile (99.8%), chlorobenzene (CB, 99.8%), diethyl ether (99.7%), DMF (99.8%) and DMSO (99.9%) were purchased from Sigma Aldrich (Korea).

2.8 Device fabrication

Fluorine-doped tin oxide (FTO) glasses (Pilkington, TEC-8, 15 Ω sq^{-1}) were etched using zinc powder and HCl solution (2 M). It was cleaned by detergent, diluted water, sonicated with acetone and isopropyl alcohol (IPA) in an ultrasonic bath for 60 min then followed by UV-O_3 treatment for 20 min. The blocking TiO_2 (Bl-TiO_2) layer was deposited on top of the FTO by spin-coating TiO_2 precursor solution (0.15 M titanium diisopropoxide bis(acetylacetonate) (75 wt% in 2-propanol, Aldrich) in 1-butanol at 2800 rpm for 20 s followed up with 125 °C for 5 min. The mesoporous titanium oxide (m-TiO_2) layer was coated on Bl-TiO_2 substrates at 2000 rpm for 20 s with 40 nm TiO_2 paste diluted in 1-butanol and annealed at 550 °C for 60 min. Finally, the substrates were immersed in 20 mM $TiCl_4$ solution at 90 °C for 10 min, then washed with DI-water and sintered at 500 °C for 30 min. The perovskite precursor solution was prepared at ambient condition in a mixed solvent of DMF and DMSO. The molar ratio for PbI_2 : MAI was fixed at 1 : 1 molar ratio. Perovskite precursor solution was spin-coated on the substrate at 4000 rpm for 25 s, 0.5 mL of diethyl ether was injected on the substrate 10 s to induce an acid–base adduct intermediate and then the film was annealed at 65 °C for 1 min to eliminate the DMSO and 100 °C for 9 min to form perovskite phase. The spin-coating procedure was performed in ambient conditions. For the preparation of the **spiro-OMeTAD** solution, 72.3 mg mL^{-1} was dissolved in chlorobenzene and spin coated with 3000 rpm for 30 s. For the new **sDTG-tpa** HTM 40 mg mL^{-1} was dissolved in CB was spin coated on the perovskite layers at 2000 rpm for 30 s. Finally, a Carbon electrode was deposited on the **spiro-OMeTAD**/**sDTG-tpa** layer.

2.9 Device characterizations

The photocurrent density–voltage (J–V) curves were measured (Oriel® Sol3A™ Class AAA solar simulator, models 94043A) at 25 °C under the AM1.5G (100 mW cm^{-2}) illumination (scan rate: 30 mV s^{-1}, both forward (from I_{SC} to V_{OC}) and reverse (from V_{OC} to I_{SC}) scan modes) adjusted using a standard PV reference cell (2 cm × 2 cm monocrystalline silicon solar cell, calibrated at NREL, Colorado, USA) and a computer controlled Keithley 2400 source measure unit. The incident photon to current conversion efficiency spectrum was measured using Oriel® IQE-200™ equipped with a 250 W quartz tungsten halogen lamp as the light source and a monochromator, an optical chopper, a lock-in amplifier, and a calibrated silicon photodetector. Prior to the use of the light, the spectral response and the light intensity were calibrated using a monosilicon detector. The single carrier space charge limited current (SCLC) method was used to calculate the mobility from the J–V curve by using the below equation,

$$J = \left(\frac{9}{8}\right)\varepsilon_0\varepsilon_r\mu_0\frac{V^2}{L^3}$$

where J, ε_0, ε_r, μ_0, V and L are current density, permittivity of free space, relative permittivity of the material, zero-field mobility, applied voltage and thickness of the organic material, respectively.

3 Results and discussion

3.1 Preparation of spirodithienogermoles

Previously, we have prepared spirobi(dithienosilole)s and spirobi(dithienogermole)s[10] and demonstrated the p-type semiconducting properties of one of them in thin film field-effect transistors.[10a] Spirodithienogermole with triphenylamine substituents **sDTG-tpa** was obtained as a yellow solid by a palladium-catalyzed Stille coupling reaction of spirobi(dibromodithienogermole) (**sDTG-Br**) with *N*,*N*-diphenyl-4-(trimethylstannyl)aniline in toluene at the reflux temperature, as shown in Scheme 1. Other spirobi(dithienogermoles) with electron-donating substituents (**sDTG-dmap** and **sDTG-mop**) were obtained in a similar manner. Their rather low isolated yields were mainly due to difficult separation from the reaction mixture that included some by-products such as partially substituted spirobi(dithienogermole)s. They are soluble in usual organic solvents like THF, toluene, and chlorocarbons, but barely soluble in methanol and ethanol. Related model compounds **m1** and **m2** were also prepared to investigate structure–property relationships. Unfortunately, these compounds could not be

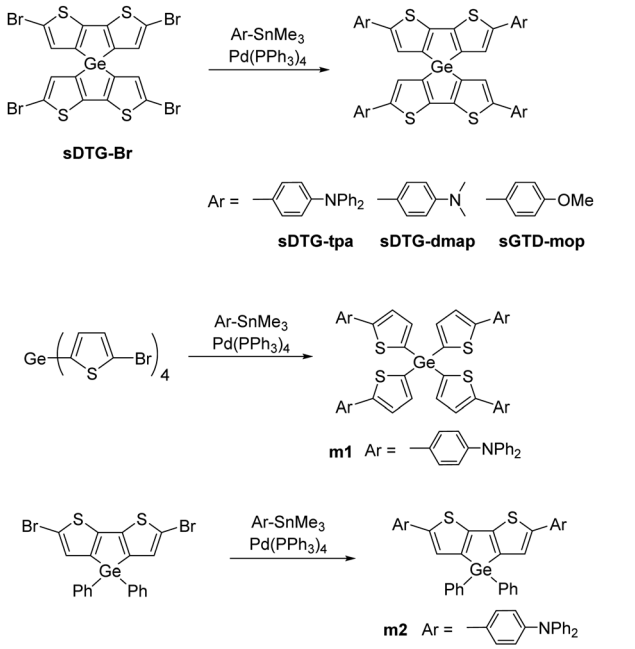

Scheme 1 Synthesis of spirobi(dithienogermole)s with electron-donating substituents and related compounds.

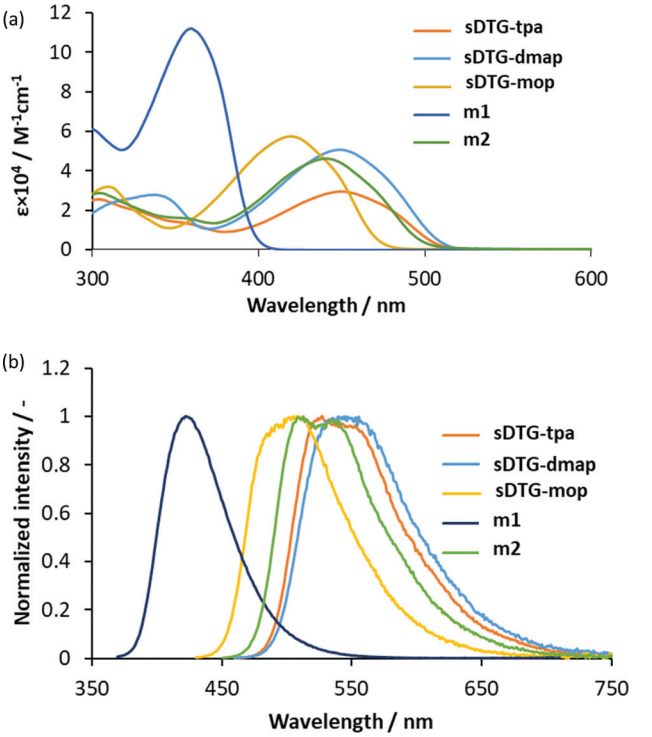

Fig. 1 UV-vis ABS at 10^{-5} M (a) and PL at 10^{-5} M (b) spectra of spiro(dithienogermole) derivatives, **m1**, and **m2**.

purified. Small signals probably due to impurities were observed in their NMR spectra, and those impurities could not be removed by silica gel, alumina, and gel permeation chromatography (Fig. S1–S5, ESI†). However, as the intensities of the unidentified signals were always low, these compounds were used for the following experiments on their optical and electrochemical properties and functionalities as HTMs in PSCs without further purification.

3.2 Optical and electrochemical properties

Fig. 1 shows UV-vis absorption (ABS) and photoluminescence (PL) spectra of these compounds. As presented in Fig. 1, the ABS maxima of the spiro compounds shifted to lower energies in the order of **spiro-OMeTAD** ≪ **sDTG-mop** ≪ **sDTG-dmap** < **sDTG-tpa**, indicating that the present DTG-based compounds should have more enhanced conjugation arising from the longer π-system. The PL bands shifted in a similar manner (**sDTG-mop** ≪ **sDTG-tpa** < **sDTG-dmap**). For compounds with triphenylamine units, both the ABS and PL maxima (λ_{max}) shifted to lower energies as **m1** (360 nm) < **m2** (441 nm) < **sDTG-tpa** (450 nm), suggesting the effects of the germanium bridge in enhancing the conjugation presumably because of the enhanced planarity. It is also likely that the spiro conjugation operates to further enhance the conjugation of **sDTG-tpa**, as previously reported for other spirobi(dithienosilole)s and spirobi(dithienogermole)s.[10] The HOMO and LUMO energy levels of those compounds were estimated on the basis of the anodic onset potentials in their cyclic voltammograms (CVs) and optical band gaps (Table 1 and Fig. S6, ESI†) together with those of **spiro-OMeTAD**.[11,12] Compounds **sDTG-tpa** and **sDTG-dmap** possess high lying HOMO compared with **spiro-OMeTAD**, likely reflecting the electron-donating properties of the thiophene rings and the expanded conjugation with aminophenyl units. Methoxy compound **sDTG-mop** showed less extended conjugation with lower-lying HOMO compared to amino compounds **sDTG-tpa** and **sDTG-dmap**, likely due to the methoxy lower electron donating properties. As conjugation length depends on the system planarity, we carried out DFT calculations on **sDTG-tpa** at the B3LYP/6-31G(d,p) level of theory (Gaussian 09, Revision A02) and the optimized geometry is presented in Fig. 2. It was found that the DTG units possess high planarity as evidenced by the endo cyclic C═C–C═C dihedral angles ranging from 0.03° to 0.06°. The DTG and adjacent phenylene units are twisted slightly with the C═C–C═C dihedral angles of 25.4–25.6°, suggesting possible conjugation between them. Indeed, the HOMO and

Table 1 Optical data in THF and HOMO and LUMO energy levels of spiro(dithienogermole) derivatives, **m1**, and **m2**, together with literature data of **spiro-OMeTAD**

Comp.	UV-vis ABS λ_{max}/nm (ε/(M cm)$^{-1}$)	PL λ_{max}/nm	HOMO /eV[a]	LUMO /eV[a]
sDTG-tpa	450 (30 000)	517, 526	−4.95	−2.62
sDTG-dmap	449 (51 000)	545	−4.74	−2.37
sDTG-mop	420 (57 000)	508	−5.12	−2.62
m1	360 (72 000)	423	−5.26	−2.29
m2	441 (1 12 000)	513	−4.99	−2.56
spiro-OMeTAD	395[b]		−5.22[c]	−2.2[c]

[a] Derived from anodic onset potentials in CVs in DMF containing TBAP as the supporting electrolyte and optical band gaps. [b] In chlorobenzene. Ref. 11. [c] Ref. 12.

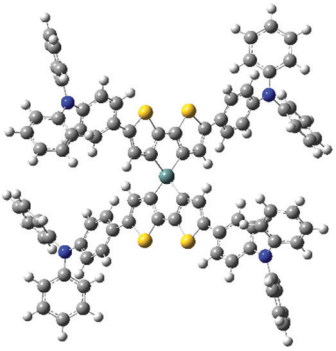

Fig. 2 Optimized geometry of **sDTG-tpa**, derived from DFT calculations at B3LYP/6-31G(d,p).

LUMO are found to be delocalized to the phenylene units (Fig. S7, ESI†).

3.3 Device performance

Finally, we examined compound **sDTG-tpa** as the HTM for PSCs. The device structure was FTO/TiO_2/$CH_3NH_3PbI_3$/HTM/carbon, in which the HOMO and LUMO energy levels of **sDTG-tpa** (HTM) nicely fit the perovskite and carbon energy levels, as shown in Fig. 3a. A cross-sectional SEM image of the device with **sDTG-tpa** is presented in Fig. 3b, revealing the multi-layered structure with finely controlled thicknesses and clear interfaces without any defects, such as pinholes of the layers. Fig. 3c shows the current density–voltage (*J*–*V*) curves using a simulated solar illuminator with the intensity of 100 mW cm^{-2}. The device with **sDTG-tpa** showed almost no hysteresis and nearly the same curve on the forward and reverse scans with high PCEs of 14.44% and 14.67%, respectively (Table 2). That the device with **sDTG-tpa** demonstrated *J*–*V* loops without noticeable hysteresis indicates that the **sDTG-tpa** structure formed constant intimate contact with the absorbing layer, thus holes have been efficiently extracted, preventing parasitic ion accumulation at the interface.[13] The external quantum efficiency (EQE) spectrum of the device showed a broad band with the maximum EQE of nearly 80% at around 400 nm, agreeing with the high PCE of the PSC (Fig. 3d). The device consistency was evaluated by *J*–*V* measurements at the voltage of maximum power point, which showed that PCE reached a steady state after 5 s, retaining it at least up to 60 s (Fig. 3e). Fig. 3f shows the high reproducibility of the fabrication of individual 10 devices.

PSC with the same structure but having **spiro-OMeTAD** as the HTM was also fabricated and its measurement data are included in Fig. 3c–f and Table 2. The results clearly indicated the superior performance of the device with **sDTG-tpa** compared with that with **spiro-OMeTAD**. Stability check of the non-capsulated devices was also performed in the dark in ambient atmosphere (humidity = 28 ± 2.2%, rt, in air), and the device with **sDTG-tpa** exhibited longer stability than that with **spiro-OMeTAD**, namely, the PCE value remained higher than 10% until experiment day 20 (Fig. 3g). To elucidate the origin of the high performance of **sDTG-tpa** as HTM compared with **spiro-OMeTAD**, we measured the hole mobilities of **sDTG-tpa** and **spiro-OMeTAD** films using the space-charge limited current method on hole-only devices whose structure is shown in Fig. 4a. As presented in Fig. 4b, **sDTG-tpa** film provided

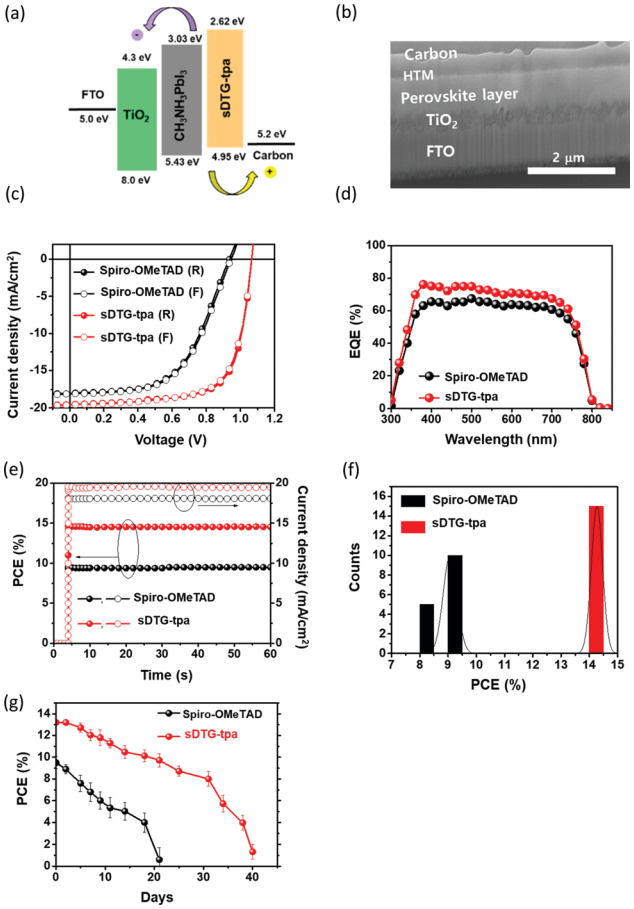

Fig. 3 Energy level diagram (a); cross-sectional SEM image of PSC with sDTG-tpa as HTM (b); and *J*–*V* curves (c), EQE spectra (d), PCE steady state (e), histogram of PCEs (f), and stability check (g) of PSCs with sDTG-tpa and spiro-OMeTAD as HTMs.

Table 2 Photovoltaic properties of PSCs with different HTMs

HTM	Scan mode[a]	V_{OC}/V	J_{SC}/mA cm^{-2}	FF/%	PCE/%	Integrated J_{SC}/mA cm^{-2}	R_S/Ω cm^{-2}	R_{sh}/Ω cm^{-2}
spiro-OMeTAD	F	0.93	18.06	55.65	9.40	18.21	9.57	1.8×10^5
spiro-OMeTAD	R	0.94	18.11	55.68	9.53	18.29	9.50	2.1×10^5
sDTG-tpa	F	1.06	19.60	69.22	14.44	19.86	4.66	2.5×10^7
sDTG-tpa	R	1.06	19.58	70.34	14.67	19.97	4.36	4.3×10^7

[a] F: forward, R: reverse.

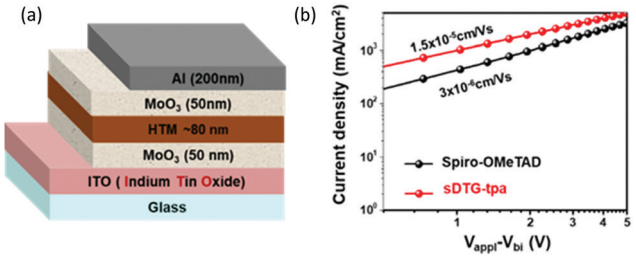

Fig. 4 Structure (a) and *J*–*V* plots (b) of hole-only devices with **sDTG-tpa** and **spiro-OMeTAD** as HTMs.

approximately five times higher mobility of 1.5×10^{-5} cm V^{-1} s^{-1} than **spiro-OMeTAD** (3×10^{-6} cm V^{-1} s^{-1}).

To know more about the different performance of PSCs based on **sDTG-tpa** and **spiro-OMeTAD**, we investigated the AFM morphologies of the perovskite film, and the perovskite films with **sDTG-tpa** and **spiro-OMeTAD** (Fig. 5). The rough morphology of the pure perovskite film became smooth and uniform for the composites with **sDTG-tpa** and **spiro-OMeTAD**. This is also seen in SEM image of perovskite with **sDTG-tpa** (Fig. 5d and e). As presented in Fig. 5b and c, the root mean square (RMS) roughness value of the perovskite with **sDTG-tpa** is smaller than that with **spiro-OMeTAD**, suggesting more efficient charge separation at the perovskite/HTM interface for **sDTG-tpa**-based PSC.

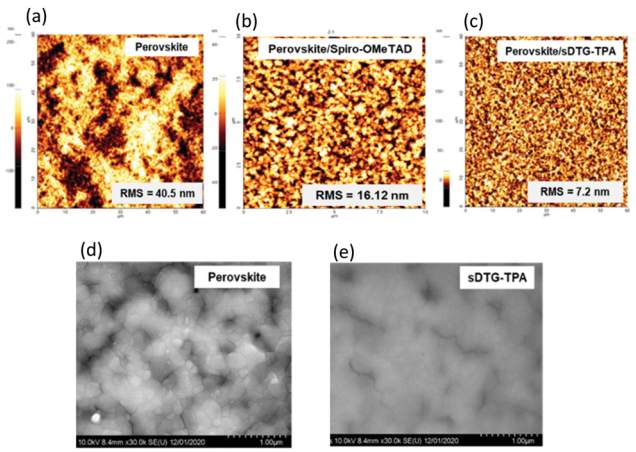

Fig. 5 AFM images and SEM of perovskite, perovskite/**spiro-OMeTAD**, and perovskite/**sDTG-tpa**.

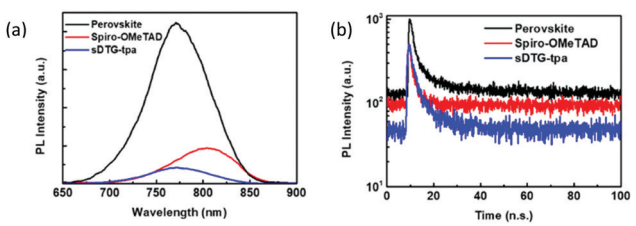

Fig. 6 Steady state PL spectra (a) and time-resolved decay profiles (b) of perovskite/**sDTG-tpa**, perovskite/**spiro-MeOTAD**, and perovskite pristine films.

Fig. 6 shows the steady state PL spectra and the time-resolved PL decay profiles for perovskite/**sDTG-tpa**, perovskite/**spiro-MeOTAD**, and perovskite pristine films. As shown in Fig. 6a, **sDTG-tpa** quenched the perovskite emission more efficiently as compared with **spiro-MeOTAD**. In addition, the perovskite/**sDTG-tpa** showed a shorter decay time of 3.4 ns than those of the perovskite/**spiro-MeOTAD** (5.2 ns) and perovskite pristine films (8.1 ns) (Fig. 6b). These are indicative of that **sDTG-tpa** has higher hole extraction ability than **spiro-MeOTAD**.

4 Conclusions

In summary, we prepared spiro(dithienogermole)s that show expanded conjugation due to high planarity and spiro conjugation. Among the presently prepared spiro compounds, that with triphenylamine substituents was examined as the HTM for PSCs and found to show improved performance compared with **spiro-OMeTAD** with respect to PSC efficiency and stability. The higher hole mobility of **sDTG-tpa** in film seems to be one of the major reasons for the higher performance as HTM. It was found that **sDTG-tpa** provided more smooth morphology of the film prepared on the perovskite film than **spiro-OMeTAD**, suggesting more efficient charge separation at the perovskite/HTM interface. Higher hole extraction ability of **sDTG-tpa** than that of **spiro-MeOTAD** was also demonstrated. These results clearly indicate the high potential of spirobi(dithienogermole)-based compounds in particular **sDTG-tpa** as dopant-free HTMs for PSCs. High planarity of the conjugated systems and effective elevation of the HOMO by introducing electron-rich thiophene and triphenylamine units seem to be responsible for the high performance of **sDTG-tpa** as HTM. PSCs with other spiro (dithienogermole) derivatives were also examined. However, the preliminary data of the devices indicated much lower efficiencies. This may be due to the molecular characteristics of these compounds. However, the reason is still unclear and further studies including optimization of device fabrication conditions seem necessary.

Conflicts of interest

There are no conflicts to declare.

Acknowledgements

This work was supported by Japan Society for the Promotion of Science (JSPS) KAKENHI (JP17H03105) and Fundamental Research Program (PNK 5840) of Korea Institute of Materials Science (KIMS).

References

1 W. Zhang, Y.-C. Wang, X. Li, C. Song, L. Wan and K. Usman, *Adv. Sci.*, 2018, **5**, 1800159.

2 (*a*) E. H. Jung, N. J. Jeon, E. Y. Park, C. S. Moon, T. J. Shin, T.-Y. Yang, J. H. Noh and J. Seo, *Nature*, 2019, **567**, 511; (*b*) N. J. Jeon, H. Na, E. H. Jung, T.-Y. Yang, Y. G. Lee, G. Kim, H.-W. Shin, S. Il Seok, J. Lee and J. Seo, *Nat. Energy*, 2018, **3**, 682–689; (*c*) H. Kwon, S. S. Reddy, V. M. Arivunithi, H. Jin, H.-Y. Park, W. Cho, M. Song and S.-H. Jin, *J. Mater. Chem. C*, 2019, **7**, 13440; (*d*) K. Gao, B. Xu, C. Hong, X. Shi, H. Liu, X. Li, L. Kie and A. K.-Y. Jen, *Adv. Energy Mater.*, 2018, **8**, 1800809; (*e*) K. Gao, Z. Zhou, B. Xu, S. B. Jo, Y. Kan, X. Peng and A. K.-Y. Jen, *Adv. Mater.*, 2017, **29**, 1703980.

3 Z. Hawash, L. K. Ono and Y. Qi, *Adv. Mater. Interfaces*, 2018, **5**, 1700623.

4 W. Zhou, Z. Wen and P. Gao, *Adv. Energy Mater.*, 2018, **8**, 1702512.

5 M. Franckevičius, A. Mishra, F. Kreuzer, J. Luo, S. M. Zakeeruddin and M. Grätzel, *Mater. Horiz.*, 2015, **2**, 613.

6 *Main Group Strategies towards Functional Hybrid Materials*, ed. T. Baumgartner, F. Jäkle, Wiley, 2018.

7 (*a*) J. Chen and Y. Cao, *Macromol. Rapid Commun.*, 2007, **28**, 1714; (*b*) J. Ohshita, *Macromol. Chem. Phys.*, 2009, **210**, 1360; (*c*) S. A. Ponomarenko and S. Kirchmeyer, *Adv. Polym. Sci.*, 2009, **235**, 33; (*d*) Y. Li, *Acc. Chem. Res.*, 2012, **45**, 723; (*e*) S. Parke, M. Boone and E. Rivard, *Chem. Commun.*, 2016, **52**, 9485; (*f*) J. Ohshita, *Org. Photon. Photovoltaics*, 2016, **4**, 52.

8 J. Ohshita, M. Miyazaki, F.-B. Zhang, D. Tanaka and Y. Morihara, *Polym. J.*, 2013, **45**, 979.

9 K. Narayanaswamy, B. Yadagiri, T. H. Chowdhury, T. Swetha, A. Islam, V. Gupta and S. P. Singh, *Chem. – Eur. J.*, 2019, **25**, 16320.

10 (*a*) J. Ohshita, K.-H. Lee, D. Hamamoto, Y. Kunugi, J. Ikadai, Y.-M. Kwak and A. Kunai, *Chem. Lett.*, 2004, **33**, 892; (*b*) K.-H. Lee, J. Ohshita, D. Tanaka, Y. Tominaga and A. Kunai, *J. Organomet. Chem.*, 2012, **710**, 53.

11 S. Wang, W. Yuan and Y. S. Meng, *ACS Appl. Mater. Interfaces*, 2015, **7**, 24791.

12 J. J. López, W. Cambarau, L. Cabau and E. Palomares, *Sci. Rep.*, 2017, **7**, 6101.

13 N. Drigo, C. Roldan-Carmona, M. Franckevičius, K.-H. Lin, R. Gegevičius, H. Kim, P. A. Schouwink, A. A. Sutanto, S. Olthof, M. Sohail, K. Meerholz, V. Gulbinas, C. Corminboeuf, S. Paek and M. Khaja Nazeeruddin, *J. Am. Chem. Soc.*, 2020, **142**, 1792.